Mechanical Systems and Signal Processing (1996) **10**(3), 293–317

DETERMINATION OF FREQUENCY RESPONSE FUNCTIONS FROM RESPONSE MEASUREMENTS—I. EXTRACTION OF POLES AND ZEROS FROM RESPONSE CEPSTRA

Y. Gao and R. B. Randall

School of Mechanical and Manufacturing Engineering, *University of New South Wales*, *Sydney* 2052, *Australia*

(*Received March* 1995, *accepted September* 1995)

In the current investigation a procedure is proposed to extract poles and zeros of transfer functions from response vibrations. In this procedure use is made of the deconvolution properties of cepstral analysis, that is, in the cepstrum domain, source and path effects are not only additive but also separated into different quefrency regions. The source effect is excluded and the complex or differential cepstra of the path are curve-fitted to extract poles and zeros. The Levenberg–Marquardt and Ibrahim time domain methods are adapted for the curve-fitting purpose. In the Levenberg–Marquardt method path dominated complex or differential cepstra (after the source effect is removed) are curve-fitted to their corresponding analytical expressions, while in the Ibrahim time domain method differential cepstra are treated as free response data. The advantages and disadvantages of the two methods are compared. The validation of this procedure is demonstrated by using the response of a free–free beam to impact and double impact excitations.

1. INTRODUCTION

Since Bogert, Healy and Tukey reported the cepstrum procedure for detection of echoes in time series, various cepstral techniques and cepstrum-based algorithms have been developed in many different research fields [1–15]. One of the first applications of cepstral techniques to the separation of source and transmission path effects was in speech analysis [16]. In the cepstrum domain, the voiced and unvoiced speech can be recognised by the presence or absence of rahmonics (periodic impulses in the cepstrum, corresponding to periodic structure in the log spectrum). The rahmonic intervals (or time interval from the origin to the first rahmonic) determine the voice pulse period. The transfer function (TF) of the vocal tract can be obtained by low-pass or comb liftering (filtering in the cepstrum domain) the corresponding cepstrum to remove the voice effects, and then forward transforming it back to the frequency domain.

Cepstral techniques have also been found very useful in condition monitoring and fault diagnostics of mechanical systems, especially in the case of operating machines where periodic excitation sources exist, such as gear meshing forces, reciprocating motion of pistons etc. Compared with speech analysis where the invariant time interval is of the order of 10 ms, the invariant time of a mechanical system is generally much longer (of the order

0888–3270/96/030293 + 25 $18.00/0

of hours or even longer). The techniques used in analysis of mechanical systems have their own characteristics, though they are based on the same properties of homomorphic deconvolution and concentration of signals with 'flat' and/or periodic spectra in specific regions in the cepstrum. The following two applications are widely used in condition monitoring and fault diagnostics, (1) extraction of vibration features corresponding to given mechanical faults (component changes at some characteristic quefrencies, such as the reciprocal of bearing related frequencies) [5, 17, 18], and (2) recovery of the vibration sources and/or transmission paths [7–9, 13–15].

The following studies are some examples of the first application. Berther and Davies used the cepstrum of response vibrations to detect the double impact caused by broken check valve plates in reciprocating pumps [18]. The cepstrum of the signal tail was subtracted from that of the entire signal. The rahmonics caused by double impact were maintained while the path events were eliminated in the cepstrum difference. Kemerait enhanced gear faults by subtracting the original time series (acceleration) from that which was recovered by liftering the corresponding complex cepstrum [5]. The trend analysis of a one-stage gear box shows that the cepstral trend is more sensitive and accurate in prediction of gear failure than spectral trend and statistical analysis [2]. Randall interpreted the relationship between various classes of gear faults and quefrency components in the cepstrum domain (corresponding to the frequency components in the frequency domain) [13–15]. He also investigated the phenomena of amplitude and frequency modulations theoretically and illustrated how cepstra can be used to detect various periodic gear faults in practical applications. A very important property of the response cepstrum was demonstrated in the case of gearbox vibration, that is, that the source and transmission path phenomena are not only additive but also concentrated in different quefrency regions [15], which makes it possible to separate them from one another.

In some cases of condition monitoring and diagnostics, it is necessary to recover source and/or path phenomena. This allows more accurate prediction of mechanical failures than the aforementioned procedures [2, 3, 5, 13–15]. Furthermore, the recovered path information is also very useful in structural modification and finite element model verification. However, the recovery procedure becomes quite complicated. Lyon and co-workers proposed a windowed cepstral technique [7–9], in which the source and path phenomena are deconvolved and separated into different disjoint quefrency regions. Consequently, time weighting (quefrency liftering) is applied to remove the unwanted effects. The remaining components are transformed back to the time domain and a smoothed vibration waveform is obtained. Lyon used this procedure and recovered the source, combustion pressure of a diesel engine, from casing vibration.

Derby proposed a method which extracts the poles and zeros of a transfer function from response cepstra [4]. The method optimises the pole and zero positions of a TF in a sense of least square error between the predicted and measured cepstral sequences. The corresponding iterative solution was sought by a steepest descent algorithm [19]. A similar proposal was put forward in reference [15], that is, the measured cepstrum could be curve-fitted with a model which was represented by the poles and zeros of the transfer function and a more valid model of the transfer function could be reconstructed from those poles and zeros. This paper and its companion [20] represent the implementation of those suggestions.

In the case where the source and path dominate different quefrency sections, a time weighting operation (liftering) can be applied to remove, for example, the source and the remaining parts can be curve-fitted to the analytical expression of the path cepstrum. However, the curve-fitted quefrency sections of cepstra are not purely path dominated and

are normally contaminated by some other unfavourable effects, such as digital calculation errors, out-of-band mode contributions and the leakage from the source. So, an algorithm which can compensate for the above effects, such as an over-sized model, is to be preferred [21, 22].

Use is made of the additive and separable properties of the source and path cepstra in this paper. The response vibrations are transformed into cepstrum sequences, and the highly concentrated source cepstrum (at low quefrency and in discrete rahmonics) is liftered out by a proper liftering function. Two algorithms, Levenberg–Marquardt and Ibrahim Time Domain (ITD), are adapted and applied to curve-fit the quefrency sections dominated by the path. The poles and zeros of an FRF are extracted by the curve-fitting operation. The first method (though not applied to the differential cepstrum) has already been reported in [23], and so is only summarised here, except for new developments.

2. CEPSTRAL ANALYSIS

2.1. ANALYTICAL REPRESENTATIONS OF COMPLEX AND DIFFERENTIAL CEPSTRA

For linear vibrations the impulse response of a mechanical system can be sampled into a discrete digital sequence which is the summation of the sampled complex exponentials:

$$h(n) = \sum_{k=1}^{2N} A_k \, \mathrm{e}^{s_k n \Delta t} = \sum_{k=1}^{2N} A_k z_k^n \tag{1}$$

where N is the number of vibrational modes of the system, Δt the sampling time interval (satisfying the requirement with respect to sampling frequency), the A_k are the constants of linear combination, and n is the integer index of the discrete sequence. The Z-transform of such exponential sequences is a rational polynomial function [16], and can be factorised as:

$$H(z) = \frac{Bz^r \prod_{k=1}^{M_i} (1 - a_k z^{-1}) \prod_{k=1}^{M_0} (1 - b_k z)}{\prod_{k=1}^{N_i} (1 - c_k z^{-1}) \prod_{k=1}^{N_0} (1 - d_k z)} \tag{2}$$

where $|a_k|$, $|b_k|$, $|c_k|$ and $|d_k|$ are all less than unity. There are M_i zeros and N_i poles inside the unit circle and M_0 zeros and N_0 poles outside the unit circle, respectively. B is a real scaling factor.

For sampled sequences the complex cepstrum may be defined as the inverse Z-transform of the complex logarithm of $H(z)$ [here denoted as $\hat{H}(z)$]. On implementation of the complex cepstrum, the following facts must be considered. If B is positive in equation (2), it only contributes to the zero quefrency component. If B is negative, the phase of the spectrum is shifted by 180°. z^r represents a delay or advance of the sequence, $h(n)$. It contributes a linear phase term in ω to $j \angle H(z)$ [the imaginary part of $\hat{H}(z)$]. In practical application, the actual sign of B needs to be determined, and the linear phase term has

to be taken out in order to make $\hat{H}(z)$ periodic and continuous [16, 24]. After these facts are taken into account, the complex cepstrum, $\hat{h}(n)$, can be represented as:

$$\hat{h}(n) = \begin{cases} \log|B|; & n = 0 \\ -\sum_{k=1}^{M_i} \frac{a_k^n}{n} + \sum_{k=1}^{N_i} \frac{c_k^n}{n}; & n > 0 \\ \sum_{k=1}^{M_0} \frac{b_k^{-n}}{n} - \sum_{k=1}^{N_0} \frac{d_k^{-n}}{n}; & n < 0. \end{cases} \tag{3}$$

The differential cepstrum is defined [16, 25, 26] by:

$$\hat{h}_d(n) \triangleq Z^{-1}\left[z \frac{\mathrm{d}}{\mathrm{d}z} H(z) \right]. \tag{4}$$

Using equation (2) and the above definition, we find [26] that the analytical expression of the path differential cepstrum is:

$$\hat{h}_d(n) = \begin{cases} r & n = 0 \\ \sum_{k=1}^{N_i} c_k^n - \sum_{k=1}^{M_i} a_k^n & n > 0 \\ \sum_{k=1}^{M_0} b_k^{-n} - \sum_{k=1}^{N_0} d_k^{-n} & n < 0 \end{cases} \tag{5}$$

where r represents the phase delay.

Comparing equations (3) and (5), it can be seen that the so-defined differential cepstrum and the corresponding complex cepstrum are related by:

$$\hat{h}_d(n) = n\hat{h}(n) \tag{6}$$

except for $n = 0$.

2.2. DECONVOLUTION OF RESPONSE VIBRATIONS

The analytical expressions of the complex and differential cepstra in the last section only involve the transmission paths. In practice, the externally measured vibration signal is the convolution of the sampled unit impulse response with the sampled source signal. If the calculation of the complex and differential cepstra is carried out on the externally measured vibration signal, $x(n)$, the calculation includes a very important procedure, deconvolution, as shown in Fig. 1. This system has convolution as its input operation and addition as its output operation (in both complex and differential cepstra [16]).

2.3. SOURCE CONTRIBUTION TO RESPONSE CEPSTRA

Vibration sources with reasonably flat autospectra can be found in many practical vibration situations. This kind of source could be impulsive or random. Combustion pressure in a diesel engine is an example of an impulsive source [9], while ambient vibrations are often caused by random excitations, such as wind loads on tall buildings,

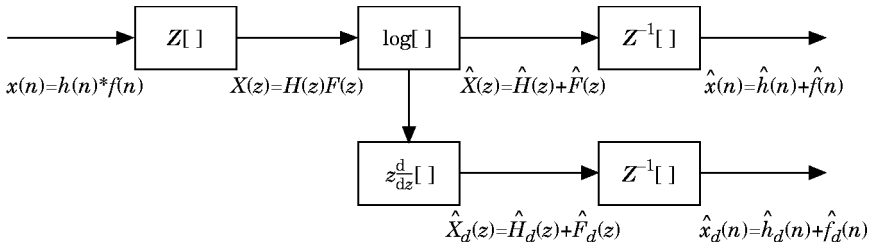

Figure 1. Source/path separation procedure, D_{1*}[ ], of cepstral analysis.

traffic excitation on bridges and wave forces on off-shore structures [27–29]. A source consisting of periodic impulses covers a wide range of vibration excitation types in operating machines. An incipient fault in a gearbox generates a repetitive impulse-like signal, while discrete faults in inner and outer races of bearings cause series of bursts [3]. The reciprocating compressor valve plate might impact the valve seat twice because of uneven wear or breakage of the plate [18]. The double impact can be considered as an impulsive source superimposed on a scaled and delayed version of itself. This source, for example, is very amenable to analysis of its contribution to the corresponding response complex cepstrum.

An impulsive source, such as the combustion pressure in an engine, can be modelled as [9]:

$$f(n) = B_0(\mathrm{e}^{-\alpha_1 n} - \mathrm{e}^{-\alpha_2 n})u(n) \tag{7}$$

where B_0 is a scaling factor, α_1 and α_2 are the parameters which adjust the waveform shape and $\alpha_1 < \alpha_2$. A double impact, for example, may be constructed by delaying and superimposing the above original impulsive source, e.g.:

$$f_1(n) = f(n) + \gamma f(n - N_0\ ) \tag{8}$$

and the corresponding complex cepstrum is [30]:

$$\hat{f}_1(n) = \begin{cases} \log|B_0(\mathrm{e}^{-\alpha_1} - \mathrm{e}^{-\alpha_2})| & n = 0 \\ \dfrac{1}{n}(\mathrm{e}^{-\alpha_1 \mathrm{n}} + \mathrm{e}^{-\alpha_2 n}) + \displaystyle\sum_{k=1}^{\infty} (-1)^{k+1} \frac{\gamma^k}{k} \delta(n - kN_0) & n > 0 \\ 0 & n < 0 \end{cases} \tag{9}$$

where $0 < \gamma < 1$. It can be shown that, in the above equation, the doubly decayed δ-function trains (with alternating sign) are caused by double impacts, while the remainder is the contribution of the original impulsive source. Figure 2 shows such an example, Fig. 2(a) is the waveform with $\gamma = 0.95$. Here, the $\mathrm{e}^{-\alpha_1}$ and $\mathrm{e}^{-\alpha_2}$ are equal to 0.7001 and 0.7, respectively. From equation (9) and Fig. 2, it can be seen that the double impact adds a periodic structure to the log spectrum, which is evenly distributed over the whole frequency band of interest, while in the cepstrum domain, this periodic structure is transformed to a train of hyperbolically and exponentially weighted impulses, rahmonics. The interval between any two adjacent rahmonics is N_0, corresponding to the number of discrete samples by which the echo is delayed.

2.4. RESPONSE CEPSTRA OF MINIMUM PHASE SYSTEMS

Equations (3) and (5) are the general expressions for the complex and differential cepstra for a linear vibration system, which includes both the positive and negative quefrency

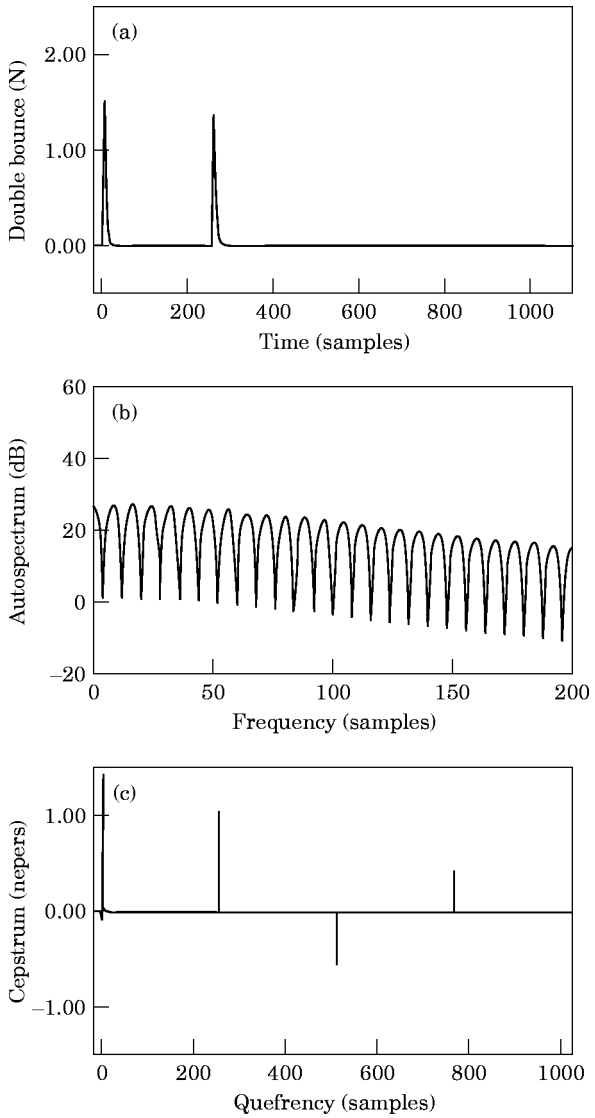

Figure 2. Contribution of double impact source.

components. We know that the negative quefrency components represent poles and zeros outside the unit circle. The former will not be present for passive stable systems, while the latter represent non-minimum phase properties. Minimum phase properties appear to apply to a wide range of passive damped mechanical structures, as in the free–free beam vibration investigated in the current research [23]. In such a case, the phase of the FRF is the Hilbert transform of the log magnitude and does not have to be measured separately [16].

Even in cases where the system under consideration has non-minimum phase properties (e.g. where the transmission path involves rotating shafts and thus a source of energy), the system can be separated into a minimum phase system and an allpass system by homomorphic filtering techniques [16]. The log magnitude of the FRF is the same as that

of the minimum phase system, while the phase of the FRF could be compensated by the phase of the allpass system.

Thus, in situations where the cepstrum is derived from the response power spectrum, the FRF phase information is lost and the derived FRF will always be 'minimum phase'. In such cases, the log magnitude of the FRF could still be derived, which is of great value diagnostically. For the above reasons, the assumption is made that the systems discussed in the following are minimum phase unless otherwise stated.

For a linear vibration of minimum phase properties, the poles of its transfer function always exist in complex conjugate pairs, while the zeros might appear in complex conjugate pairs and/or in a real form [30]. The above pole and zero patterns guarantee that the complex and differential cepstra are real discrete sequences. It has been proven that the real zeros are remote from the frequency axis, especially in the case of light damping [30, 31], meaning that their effects in the complex cepstrum die out very rapidly with quefrency. From the above arguments and equations (3) and (5), the complex and differential cepstra of the path in the regions where they dominate can be expressed just using the complex conjugate poles and zeros as:

$$\hat{h}(n) = \begin{cases} \log|B| & n = 0 \\ 2\sum_{k=1}^{N_i/2} \frac{A_{ck}^n}{n} \cos(\omega_{ck} n) - 2\sum_{k=1}^{M_i/2} \frac{A_{ak}^n}{n} \cos(\omega_{ak} n) & n > 0 \\ 0 & n < 0 \end{cases} \tag{10}$$

and:

$$\hat{h}_d(n) = \begin{cases} r & n = 0 \\ 2\sum_{k=1}^{N_i/2} A_{ck}^n \cos(\omega_{ck} n) - 2\sum_{k=1}^{M_i/2} A_{ak}^n \cos(\omega_{ak} n) & n > 0 \\ 0 & n < 0 \end{cases} \tag{11}$$

respectively, where the A_{ck} and A_{ak} represent the damping associated with the poles and zeros, and the ω_{ck} and ω_{ak} the damped natural frequencies of the poles and zeros, respectively.

Figure 3 depicts the flow chart for computational realisation of complex and differential cepstra of minimum phase systems. In this flow chart, the computation can start with discrete time data, FRF data, or even power spectrum data to cope with the situations where only one of the above types of data is available.

It should be pointed out that the operations of zero padding or smoothly extending the log magnitude spectrum are necessary and very useful. In practical computation, the FFT algorithm is used, which often requires that the data length, N, be a power of 2, while FFT analysers (such as the B&K2032 used in this investigation) output typically 801 line spectral samples, which need to be extended to at least 1024 lines. The extension could be realised by either padding zeros to the last section or smoothly extending the log spectrum in terms of its mass or spring properties [32]. On the other hand, if discrete time data are used in the computation, the length of spectral data is a power of 2, say, 1024. The log spectrum in the frequency region near π (corresponding to half the sampling frequency) might have sharply varying peaks or valleys. These peaks and valleys might be modes in which we are not interested or might be caused by aliasing or other reasons, and need to be filtered out.

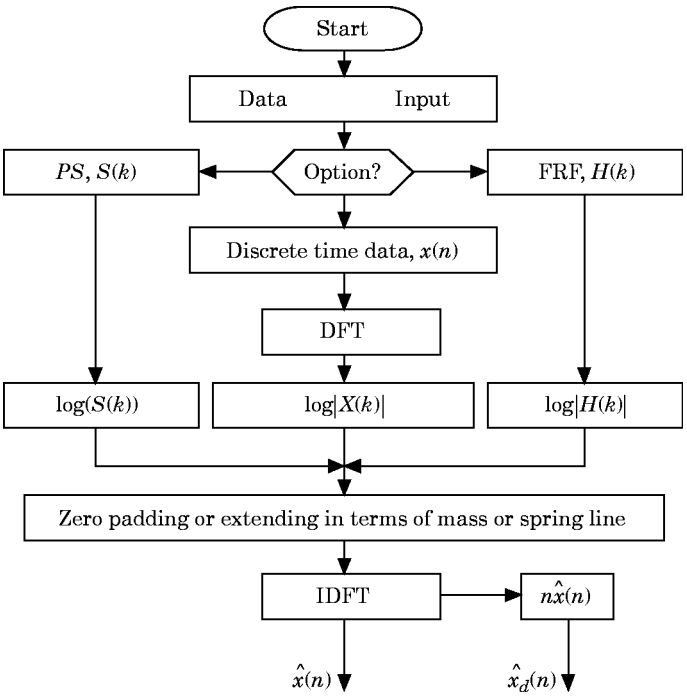

Figure 3. Computational realisation of response cepstra of minimum phase systems.

In practice, the smoothing operation can be applied to frequency components below and/or above a selected frequency band. The central frequency and width of the frequency band can be chosen according to the user's requirement. This not only makes it possible to use a smaller order of model to extract the poles and zeros from a given frequency band, but also reduces the amount of noise in the cepstrum which would result from abrupt changes in the log spectrum if a simple rectangular weighting function were used. Figure 4

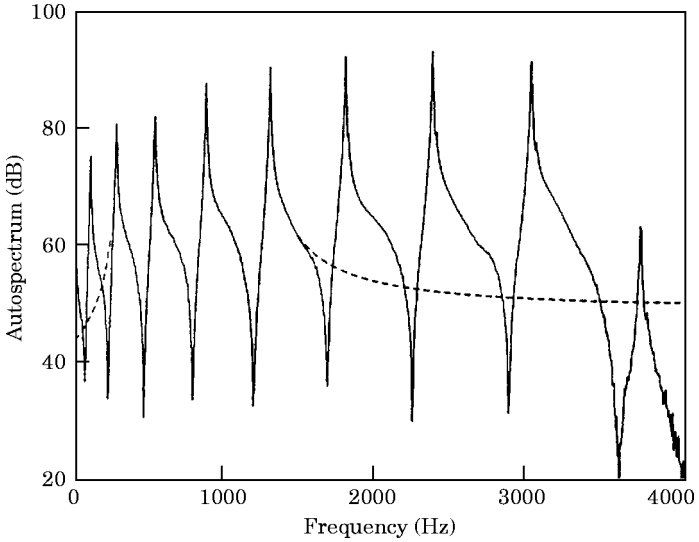

Figure 4. Smooth extension of the log spectrum.

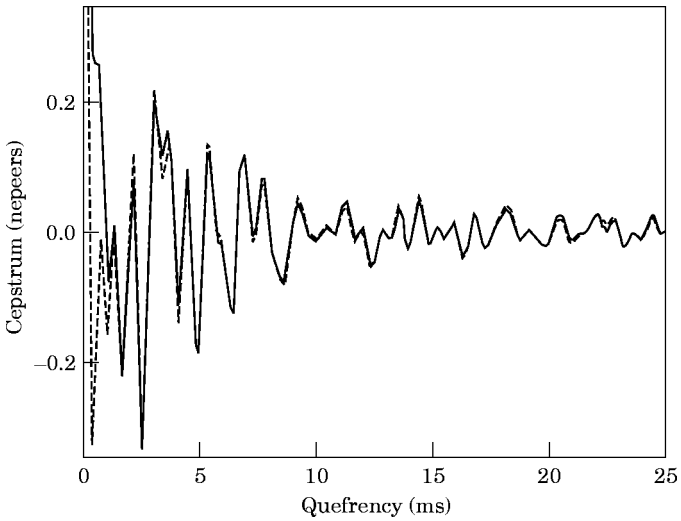

Figure 5. Comparison of complex cepstra. – – – –, corresponding to the smoothed and extended log spectrum in Fig. 4; ——, regenerated for the poles and zeros in the frequency range 248–1500 Hz.

shows an example of such an operation. The time data are the acceleration from a free–free beam (see later). The solid line is the log spectrum from 0 to π (corresponding to sample numbers 0–1023) and the dashed line is the spectrum where the smoothing operation is applied to the frequency components below 248 Hz and above 1500 Hz in terms of spring and mass properties, respectively. In Fig. 5, the dashed line is the complex cepstrum corresponding to the smoothed and extended (dashed line) log spectrum in Fig. 4; the solid line is generated using the poles and zeros in the range from 248 to 1500 Hz. The two curves correspond very well except for the very low quefrency section [30].

The differential cepstrum of a time series can be implemented alternatively by using the following equation [16, 30]:

$$\hat{x}_d(n) = \mathscr{F}^{-1}\left[\frac{\mathscr{F}[nx(n)]}{\mathscr{F}[x(n)]}\right] \tag{12}$$

in which the scaling factor, B, is lost and the zero frequency component represents the phase delay (or advance) term, z^r, in equation (2). All the functions involved in the calculation procedure are uniquely well-defined and there is no phase unwrapping required.

In the case where the measured vibration is a reasonable approximation of the impulse response of the system under measurement, calculation of differential cepstra from equation (12) has advantages over the implementation procedure depicted in Fig. 3. In the latter case, the differential cepstrum components in the high quefrency region might be distorted greatly because the corresponding complex cepstrum components in the region are greatly influenced by noise. Figure 6 compares the differential cepstra obtained by the above two different procedures. The response vibration was measured near the middle of a free–free beam (see later). The lower figure shows the differential cepstrum obtained using equation (12) and the upper one the corresponding complex cepstrum multiplied by the frequency index, n. It can be seen that the two curves correspond well in the quefrency region 0–50 ms, while in the remaining region, the upper curve does not decay with quefrency, thus indicating that it is dominated by noise.

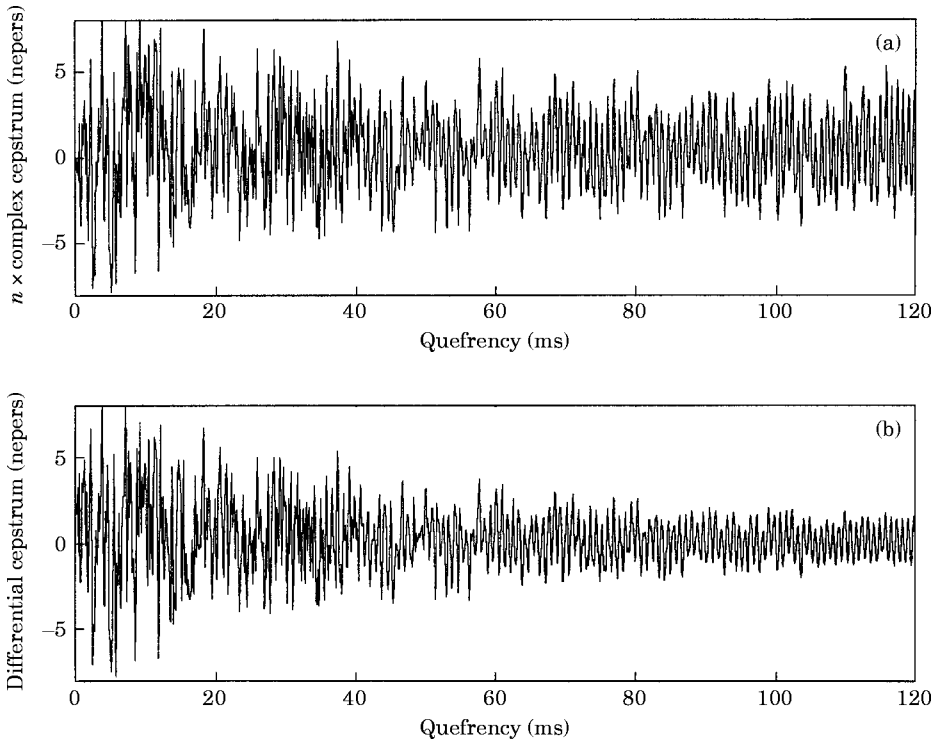

Figure 6. Comparison of (a) $n \times$ complex cepstrum and (b) differential cepstrum.

3. EXTRACTION OF POLES AND ZEROS FROM RESPONSE CEPSTRA

3.1. BASIC PRINCIPLES

In many cases, as mentioned above, the source and path phenomena are separable as well as additive. In those sections dominated by the path events, the approximations, $\hat{x}_d(n) \approx \hat{h}_d(n)$ for the differential cepstrum and $\hat{x}(n) \cong \hat{h}(n)$ for the complex spectrum could be made. By means of applying a proper lifter function (weighting function which is used to lifter out the source events) to a measured response cepstrum, the analytical expression of the path differential (or complex) cepstrum can be curve-fitted to the cepstrum of the measured response, allowing extraction of the poles and zeros of the transfer function.

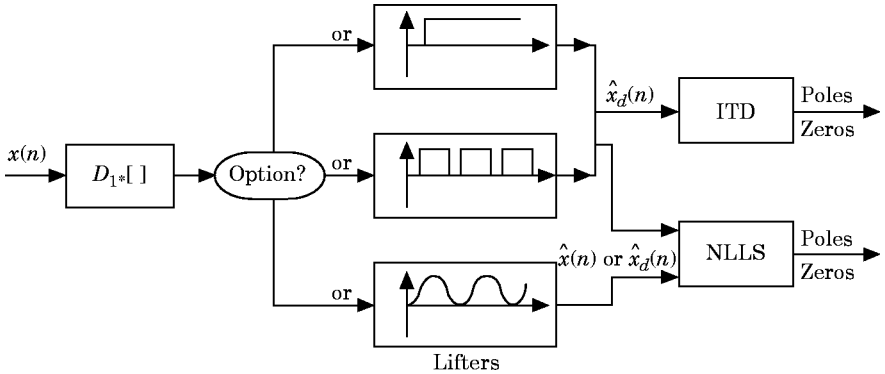

Figure 7. Flow chart extracting poles and zeros from response cepstra.

For the purposes of conciseness, the results from three typical points of the beam will be discussed in the following sections. Point 1 (at the one end of the beam) is the driving point, point 5 (close to the middle of the beam) and point 8 (at the other end) are the transfer measurement points.

3.3. NONLINEAR LEAST SQUARES (NLLS) OPTIMISATION

The NLLS algorithms arise most commonly from data fitting operations where one is trying to fit the data with a model. In our case the data could be the $\hat{x}(n)$ or $\hat{x}_d(n)$, and the model is either equation (10) or (11). The error function, for example, is the difference between the observed values, $\hat{x}(n)$, and those evaluated by the model $\hat{h}(n)$, e.g.:

$$\begin{aligned} e(\beta, n) &= \hat{x}(n) - \hat{h}(n) \\ &= \hat{x}(n) - 2\sum_{k=1}^{N_i/2} \frac{1}{n}\beta_{2k-1}^{n} \cos(\beta_{2k} n) + 2\sum_{k=1}^{M_i/2} \frac{1}{n}\beta_{P_i+2k-1}^{n} \cos(\beta_{P_i+2k} n) \end{aligned} \tag{13}$$

where the corresponding variable vector to be extracted can be constructed as:

$$\begin{aligned} \beta &= [A_{c1}, \omega_{c1}, A_{c2}, \omega_{c2}, \ldots, A_{cP_i/2}, \omega_{cP_i/2}, A_{a1}, \omega_{a1}, A_{a2}, \omega_{a2}, \ldots, A_{aM_i/2}, \omega_{aM_i/2}]^T \\ &= [\beta_1, \beta_2, \ldots, \beta_{P_i+M_i}]^T. \end{aligned} \tag{14}$$

The non-linear least squares problem consists of choosing β so that the fit is as close as possible in the sense that the sum of the squares of the errors $e(\beta, n)$ is minimised. Here, the Levenberg–Marquardt approach is recommended, as described in Appendix A. The Levenberg–Marquardt algorithm requires initial trial values of the variable vector, β, which is to be extracted and the exact order of the model function, $f(\beta, n)$, (in our case the numbers of poles and zeros). The order and the initial frequency values could often be determined from the corresponding autospectra, because the smooth and flat force autospectra (hammer impact) would not effectively affect them, or from a finite element model or previous measurement. The initial magnitudes (related to damping) of the pole and zero terms could be always set to a value very close to unity, say 0.999, especially in the case of light damping. As recommended in Dennis and Schabel [20], the above model ensures that the different elements are of the same order; with the A-values being close to unity and the ω-values falling in the range of 0–2π, which is helpful in convergence of the algorithm.

The acceleration time data were used to compute the corresponding response complex cepstrum (Fig. 3, central path). Peaks and valleys near the Nyquist frequency were smoothed out as discussed previously (Fig. 4). Before input into the curve-fitting programme, the complex cepstrum components in the initial quefrency section need to be liftered (weighted) out by applying a weighting function, such as:

$$u(n - n_0) = \begin{cases} 0 & n < n_0 \\ 1 & n \geqslant n_0 \end{cases} \tag{15}$$

to the measured response complex cepstrum, as shown in Fig. 9. The function, $u(n - n_0)$ is an effective and convenient liftering operation. It does not change the analytical expression in the curve-fitting region ($n \geqslant n_0$) and need not be built into the model function. The liftering operation can be implemented simply by starting the curve-fitting algorithm from n_0 on, which removes the adverse contribution (mainly caused by sources and truncation) from the very low quefrency section, to the NLLS algorithm.

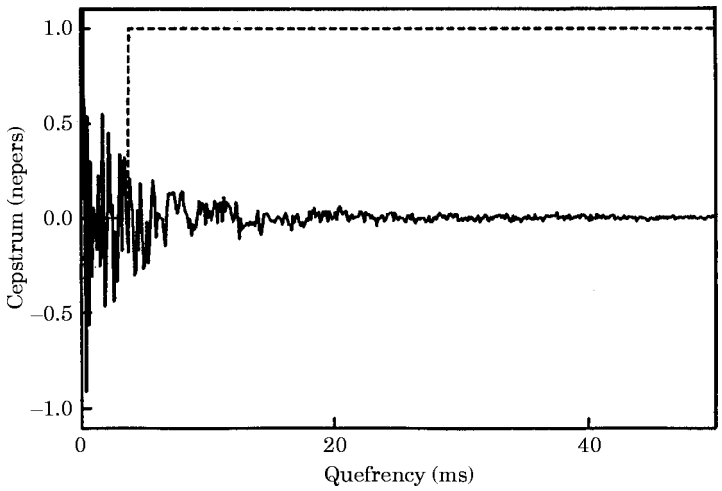

Figure 9. High pass liftering the complex cepstrum. ——, cepstrum; – – –, weighting.

Table 2 lists the poles and zeros extracted by the NLLS procedure. It can be seen that the frequencies of the poles and zeros correspond well to those obtained by the ITD Method (Table 3) as well as in terms of both the Bernoulli–Euler equation and the peaks of the corresponding FRFs (Table 1).

Figure 10 compares the complex cepstra generated from equation (10) for the curve-fitted poles and zeros listed in Table 2 with the measured ones computed from the procedure depicted in Fig. 3 (using acceleration time data). The solid curves are the regenerated ones and the dotted curves the measured ones. For all the three measurements (one driving point and two transfer measurements), the solid curves correspond well to the corresponding dotted ones, respectively, except for the deviations in the very low

TABLE 2

Poles and zeros from curve-fitting complex cepstra

Point 1	Point 5	Point 8
Poles (Hz)		
$-2.61 \pm j100.3$	$-2.64 \pm j101.0$	$-3.80 \pm j100.0$
$-3.65 \pm j274.7$	$-3.96 \pm j274.7$	$-3.65 \pm j275.2$
$-4.12 \pm j536.8$	$-3.91 \pm j536.5$	$-4.30 \pm j536.9$
$-3.58 \pm j883.4$	$-3.67 \pm j883.5$	$-3.44 \pm j883.3$
$-3.45 \pm j1311$	$-3.27 \pm j1311$	$-3.29 \pm j1311$
$-3.59 \pm j1819$	$-3.62 \pm j1819$	$-3.57 \pm j1819$
$-3.79 \pm j2404$	$-4.00 \pm j2404$	$-3.89 \pm j2404$
$-4.23 \pm j3062$	$-4.21 \pm j3062$	$-4.13 \pm j3062$
Zeros (Hz)		
$-4.06 \pm j66.23$	$-5.99 \pm j366.1$	
$-2.46 \pm j226.3$	$-1.08 \pm j1189$	
$-2.59 \pm j468.9$	$-2.96 \pm j2450$	
$-3.15 \pm j798.9$		
$-4.23 \pm j1210$		
$-4.57 \pm j1706$		
-2.50 ± 2278		
-3.38 ± 2923		

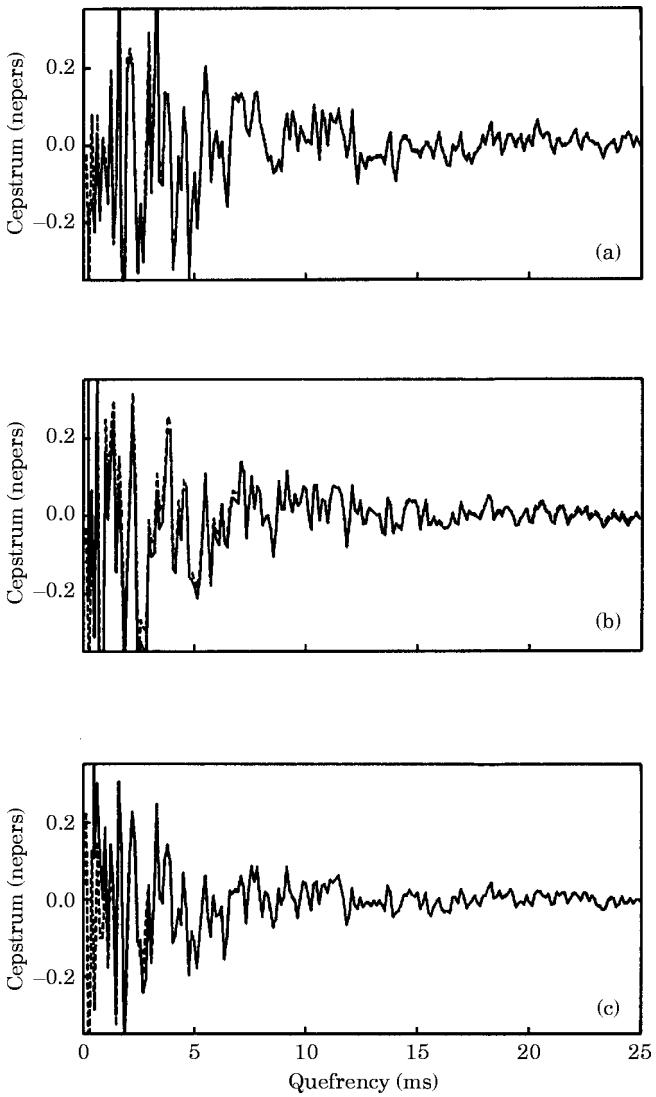

Figure 10. Comparison between the regenerated (——) and measured (– – –) complex cepstra. (a) Point 1; (b) point 5; (c) point 8.

quefrency section. This is consistent with the fact that in the case of an impulsive source, the very low quefrency section contains a mixture of path, source and some other effects (noise and truncation, etc.), and the remaining quefrency region is dominated by the complex conjugate poles and zeros.

In the curvefitting procedure, however, the complex cepstrum components are heavily weighted by the hyperbolic function, $1/n$. From the curvefitting viewpoint, it is preferable to remove such a weighting effect on the quefrency components which provide the curve fitter with information about the poles and zeros. This can be realised by curvefitting the response differential cepstrum instead of the response complex cepstrum.

Equation (6) shows that the analytical expressions of the complex and differential cepstra are related by the hyperbolic function, except for the zero frequency component. When the Levenberg–Marquardt method is used to extract the poles and zeros from the

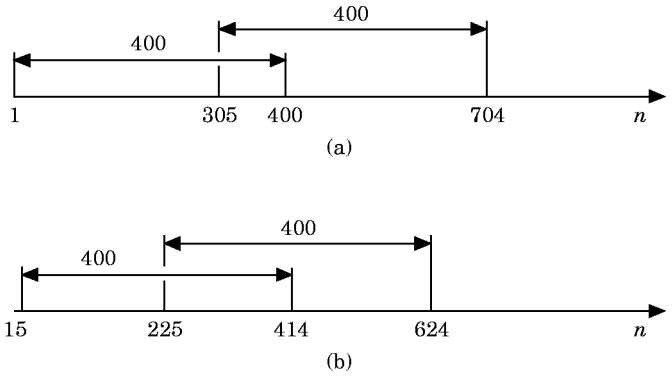

Figure 11. Two extreme positions of the quefrency regions corresponding to minimum and maximum n_0 (a) for the response differential cepstrum and (b) for the response complex cepstrum.

differential cepstrum, the variable vector to be extracted is the same as in equation (14), however, the model function should be replaced by equation (11).

The transfer measurement at point 5 on the free–free beam was used to investigate the properties of the NLLS method in curvefitting the response complex and differential cepstra. Here, the response differential cepstrum was computed according to equation (12), rather than by multiplying the corresponding complex cepstrum by the quefrency index n.

An investigation has been made of the position of the quefrency region from which all the eight poles and three zeros (within the frequency band 0–3200 Hz) of the transfer measurement at point 5 could be extracted correctly. The initial values of the variable vector to be extracted were set to the same values for all the calculations. The data length to be curve fitted was chosen as 400, and the starting point n_0 [equation (15) and Fig. 9] of the curvefitted quefrency region was increased in steps of five from the very beginning. Under the above conditions, it was found that the range of n_0 was 1–305 for curvefitting the differential cepstrum, and 15–225 for curvefitting the complex cepstrum, respectively, meaning that a wider range of quefrency regions can be used to extract poles and zeros if the weighting by the hyperbolic function $1/n$ has been avoided. Figure 11 illustrates the

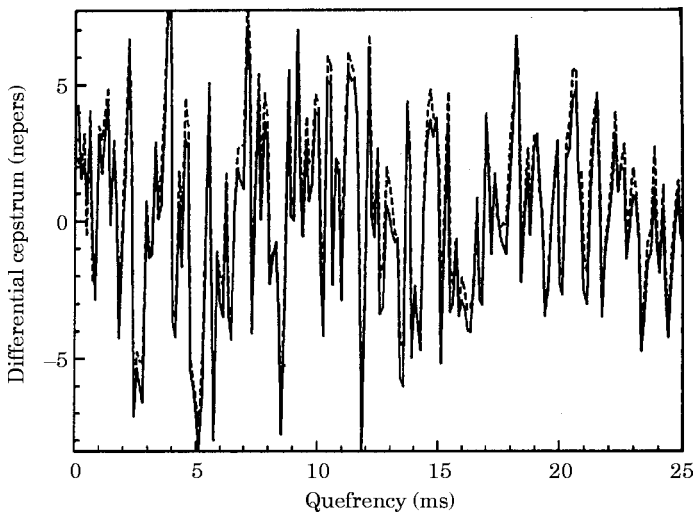

Figure 12. Comparison between the regenerated (——) and measured (– – –) differential cepstra.

range of the two extreme quefrency regions corresponding to minimum and maximum n_0 for curvefitting both the complex and differential cepstra, respectively.

Figure 12 shows the differential cepstrum (solid line) generated from the curve-fitted poles and zeros and the measured one (dashed line) using acceleration time data. The correspondence between them is obvious, even in the very low quefrency region. This implies that the contamination to the very low frequency region caused by the impulsive source and out-of-band modes is reduced in the differential cepstrum.

3.4. THE IBRAHIM TIME DOMAIN METHOD

The ITD method has been specially designed to deal with free decay response data [21, 33–35]. Equation (11) shows that the differential cepstrum has the same form as a free decay response. By treating differential cepstrum sequences as free decay responses we can adapt the ITD method to extract poles and zeros from them [30, 36].

TABLE 3

Parameters identified in a typical run of ITD program

				Eigenvectors		
f(Hz)	ζ (%)	$\Delta\varphi$ (deg)	|MSCCF|	Point 1	Point 5	Point 8
Poles						
101.2	5.462	0.008	0.999	0.956	1.000	0.959
275.5	2.467	0.021	0.999	1.000	0.958	0.995
537.6	1.014	0.051	0.999	0.980	1.000	0.990
883.6	0.502	0.055	1.000	0.990	1.000	1.000
1311	0.279	0.018	0.999	1.000	1.000	1.000
1821	0.121	0.196	0.994	0.967	1.000	0.996
2407	0.137	0.071	0.998	0.989	1.000	0.979
3065	0.199	0.119	1.000	0.980	0.970	1.000
Zeros						
71.32	18.66	0.161	0.996	1.000	0.226	0.105
226.9	1.611	0.039	1.000	1.000	0.028	0.030
372.7	2.389	0.047	0.999	0.019	1.000	0.023
469.2	1.116	0.008	0.999	1.000	0.024	0.025
799.8	0.581	0.039	1.000	1.000	0.016	0.014
1187	0.201	0.001	1.000	0.157	1.000	0.008
1210	0.675	0.028	0.996	1.000	0.026	0.027
1708	0.632	0.429	0.997	1.000	0.018	0.020
2280	0.125	0.224	1.000	1.000	0.015	0.006
2450	0.094	0.161	0.999	0.060	1.000	0.053
2923	0.321	−0.004	0.991	1.000	0.052	0.006
Noise modes						
93.58	95.86	0.319	0.902			
157.0	65.89	1.120	0.957			
371.2	15.74	0.184	0.977			
389.7	57.97	1.42	0.876			
872.3	32.14	12.02	0.829			
1013	32.85	9.991	1.000			
1295	33.76	16.19	0.850			
2167	2.209	−1.559	0.752			
2477	2.071	7.451	0.832			
2547	1.388	7.736	0.768			
2946	2.608	−0.744	0.781			
3087	0.914	0.894	0.975			

Usually, an oversized ITD model is used to provide an outlet for various types of noise contained in the measured free response data. The use of the oversized model eliminates the need to determine the exact number of modes excited, but gives rise to the problem of distinguishing the true physical modes from noise (or computational) ones. The modal confidence factor (MCF) was used first for the above purpose [21]. The MCFs have to be inspected both for each measurement point and mode by mode. The overall modal confidence factor (OAMCF) compresses the above confidence information for each mode [22]. We have found it useful to use another distinguishing factor, the mode shape coherence and confidence factor (MSCCF), introduced in Gao [30, 37–39], to separate the true physical modes from computational (noise) modes. The MSCCF is defined as:

$$\text{MSCCF} \triangleq \frac{\{\psi_k^u\}^T\{\psi_k^l\}^* \, e^{s_k \Delta t_3}}{\{\psi_k^l\}^T\{\psi_k^l\}^*} \quad k = 1, 2, \ldots, 2N \tag{16}$$

where $\{\psi_k^u\}$ and $\{\psi_k^l\}$ represent the upper and lower halves of the k-th eigenvector, $\{\psi_k\}$, respectively, and Δt_3 the time shift between $\{\psi_k^u\}$ and $\{\psi_k^l\}$. The superscripts, * and T stand for complex conjugate and matrix transpose, respectively. It has been found that the MSCCF has the ability to distinguish three kinds of modes, true physical modes within the frequency range (0–f_π), frequency folded and/or overlapped ones and computational (noise) ones. This ability makes it possible to zoom eigenvalue positions in the Z-plane. Further details can be found in [30].

3.4.1. *Experimental results from the free–free beam*

The three differential cepstra corresponding to the three measurements mentioned before were treated as three 'free responses' obtained at the same time and entered into the ITD identification program. Table 3 lists the identified results (with $|\text{MSCCF}| > 0.7$) obtained from a typical run of the ITD program. Analysis parameters are given at the bottom of the table. Here NDOF and NCOL specify the number of rows and columns of the two response matrices in the ITD method, and I_1 and I_3 represent the number of samples delay between the two matrices and between their upper and lower halves, respectively [30]. The chosen parameters do give frequency folding, and thus zoom in the Z-plane, but the phase of the MSCCFs given in the table has been normalised for convenience of assessment [30]. In the table, the identified 'modes' have been collected into three groups, viz. true poles, true zeros, and computational modes. Nineteen computational modes had already been eliminated by the above-mentioned test on |MSCCF|.

The true physical poles and zeros correspond well with the results obtained using the NLLS optimisation procedure (Table 2) as well as the corresponding frequencies read off directly from the measured FRFs and calculated in terms of the Bernoulli–Euler equation (Table 1).

From Table 3 it can be seen that all the true physical poles and zeros have a very high modal coherence and confidence information. Among them the minimum value of |MSCCF| is 0.994, and the maximum phase deviation is 0.429°. The requirement that the MSCCF should condense to e^{j0} (after phase normalisation [30]) is a necessary but not a sufficient condition for the mode to be identified accurately and in this analysis all true physical poles and zeros satisfied this necessary condition, though some of the noise or computational modes might be incorrectly distinguished as true modes. Looking at the computational modes in more detail, it is seen that setting the minimum value of |MSCCF| at 0.95 eliminates all the noise modes except those at 157.0, 371.2, 1013 and 3087 Hz, and further restriction of the maximum phase deviation $\Delta\varphi$ to 1°, leaves only 371.2 and 3087 Hz. Actually, all the computational modes can be eliminated by inspecting the variation of eigenvalue positions in the S-plane in multiple runs of the ITD identification

program using different free decay data segments and/or different analysis parameters [40]. For physical modes their positions should converge, while for noise or computational modes their positions would be random in multiple runs of the ITD program. In this case, changing the value of I_1 (the number of samples delay between the two matrices) eliminated the two remaining noise modes.

Table 4 lists the damping ratios and natural frequencies for the first five poles which are extracted by the ITD method from the response differential cepstra, the NLLS from the response complex cepstra and curve-fitting the FRFs, respectively [30]. Excellent correspondence can be found between the natural frequencies identified by ITD method with I_1 increasing from 1 to 6 and those extracted by the FRF curvefitting and NLLS procedures. The significance is that when I_1 is increased from 1 to 6, the corresponding damping ratios tend to be more comparable with the corresponding ones identified by the other two methods.

3.4.2. *Distinguishing between poles and zeros*

From equations (11) it can be seen that the differential cepstrum is a linear combination of pole and zero terms, the only difference being that they have opposite sign (positive for poles and negative for zeros). Solution of the eigenvalue problem in the ITD method gives vectors with an unknown scaling constant, so the sign of the various terms cannot be determined directly. However, if more than one measurement is available as in the case described here, the multi-point differential cepstra can be treated as multi-point free decay responses, and the corresponding pseudo mode shapes [ψ] offer very useful information about whether individual eigenvalues represent poles or zeros. This is because poles are global properties, whereas zeros are different for different measurement points. Table 3 also lists the magnitudes of the eigenvectors corresponding to the valid 'modes' in it. These are normalised in each case by scaling the largest value to unity. Note that there is a difference in this respect between the differential cepstrum and the impulse responses corresponding to ordinary modes, in that there is not a separate scaling constant or residue for each 'mode' in the mode summation formula of equation (11). The question is whether a component is present, in which case it will have a normalised value close to unity, or not present, in which case it will have a normalised value close to zero. Thus the poles are expected to be present at all measurement points (except perhaps where there is a node in a particular mode shape), while the zeros should only be present in the measurement

TABLE 4

Comparison of the first five poles obtained by different methods

	ITD						
	$I_1 = 1$	$I_1 = 2$	$I_1 = 3$	$I_1 = 4$	$I_1 = 6$	Fitting FRF	NLLS
ζ (%)	4.19	4.15	3.55	3.62	2.55	2.83	2.61
f (Hz)	101.2	102.3	101.8	101.7	101.1	100.7	100.3
ζ (%)	1.61	1.77	1.72	1.62	1.74	1.36	1.32
f (Hz)	276.7	276.4	276.2	276.2	276.1	275.3	274.7
ζ (%)	0.995	0.986	0.993	0.919	0.896	0.788	0.766
f (Hz)	537.0	537.8	537.6	537.6	537.6	537.1	536.8
ζ (%)	0.649	0.461	0.444	0.433	0.407	0.367	0.405
f (Hz)	883.4	883.5	883.3	883.4	883.4	883.2	883.4
ζ (%)	0.227	0.208	0.211	0.188	0.202	0.233	0.260
f (Hz)	1311	1311	1311	1311	1311	1311	1311

to which they apply. From the information in Table 3 it can be seen that all poles had eigenvector components close to unity (>0.956) in all measurements, while the zeros had a value of unity in one measurement only, and values close to zero (<0.226) in the other two. It was thus not difficult to distinguish poles from zeros, and assign the zeros to the particular measurement point to which they apply.

4. EXCITATION WITH A DOUBLE IMPACT

In this section, the case is considered where the forcing function is not a simple impact but a double impact as this gives a similar result to both repeated and periodic forcing functions. Figure 13 shows the driving point response autospectrum and illustrates that because of the superimposed ripple caused by a double impact on the beam, it is no longer so simple to read the system poles and zeros as in the case of single impact.

The double impact contributes a series of equally-spaced and sign-alternating rahmonics at higher quefrencies to the response complex cepstrum. The spacing can be determined either by inspection from the cepstrum (most accurately from the highest rahmonic present) or from a knowledge of the delay or periodic time. As shown in Fig. 7, the rahmonics could be removed using either an appropriate sine squared weighting function or a comb lifter. The sine squared weighting function [(Fig. 14(a)] does change the analytical expression in the quefrency regions dominated by the path cepstrum and should be built into the model, $\hat{h}(n)$, on using the NLLS procedure, meaning that both the error function, equation (13), and the Jacobian matrix (Appendix A), have to be multiplied by the weighting function in the curve-fitting procedure. However, the comb lifter [Fig. 14(b)] does not affect the analytical expression in the regions dominated by the path cepstrum and need not be built into the model on using the NLLS procedure. Its effects are treated simply as noise.

Figure 15 compares the cepstrum (dashed curve) generated by equation (10) for the poles and zeros extracted in this way with that (solid curve) of the measured FRF without double

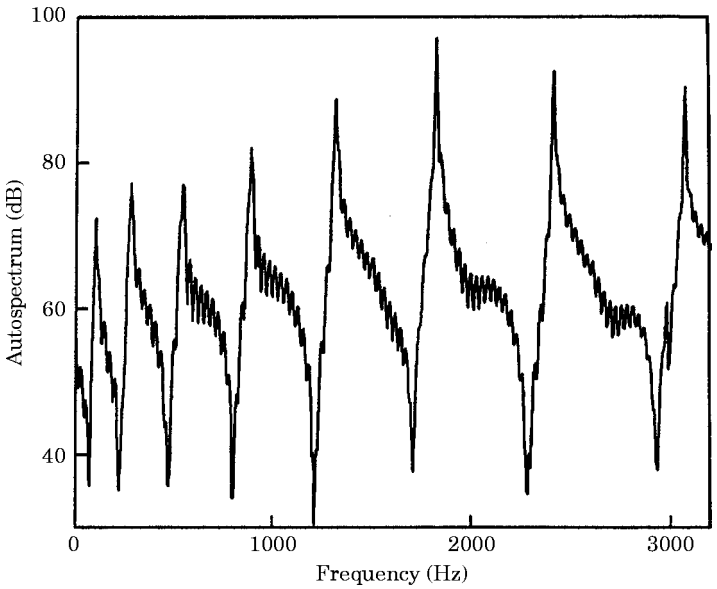

Figure 13. Driving point response autospectrum (acceleration) for point 1 with double impact in excitation (dB re 10^{-3} m/s^2).

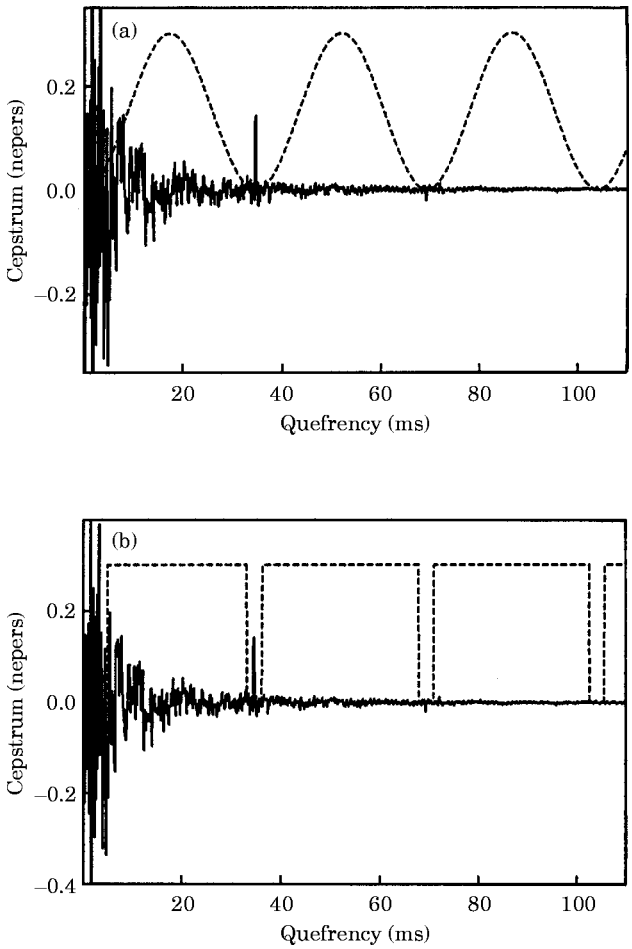

Figure 14. Driving point response complex cepstrum (acceleration) for point 1 with double impact in excitation. (a) Sine squared weighting function; (b) comb weighting function. ——, Cepstrum; – – –, weighting.

impact. From this figure, very good correspondence can be found between the two curves for both the sine squared weighting function [Fig. 15(a)] and the comb weighting function [Fig. 15(b)].

The sine squared weighting function would be difficult to apply with the ITD method, so the comb weighting function was tried. Accordingly, as shown in Fig. 16, the differential cepstrum is simply set to zero between zero crossings on either side of each rahmonic, so as to reduce the amount of 'noise' to be coped with.

Figure 17 compares the FRFs regenerated using the curve-fitted poles and zeros from the improved ITD method and the NLLS method with a direct measurement (without double impact). Note that these results are for a driving point measurement, so no "phantom zeros" [12, 30] have been included, but the indication is that the improved ITD method gives results comparable to those obtained by the NLLS curvefitting method. To obtain a better match at high frequencies, and in transfer measurements, it would be necessary to include appropriate "phantom zeros" [12, 30], but in this respect there is no difference between the two techniques.

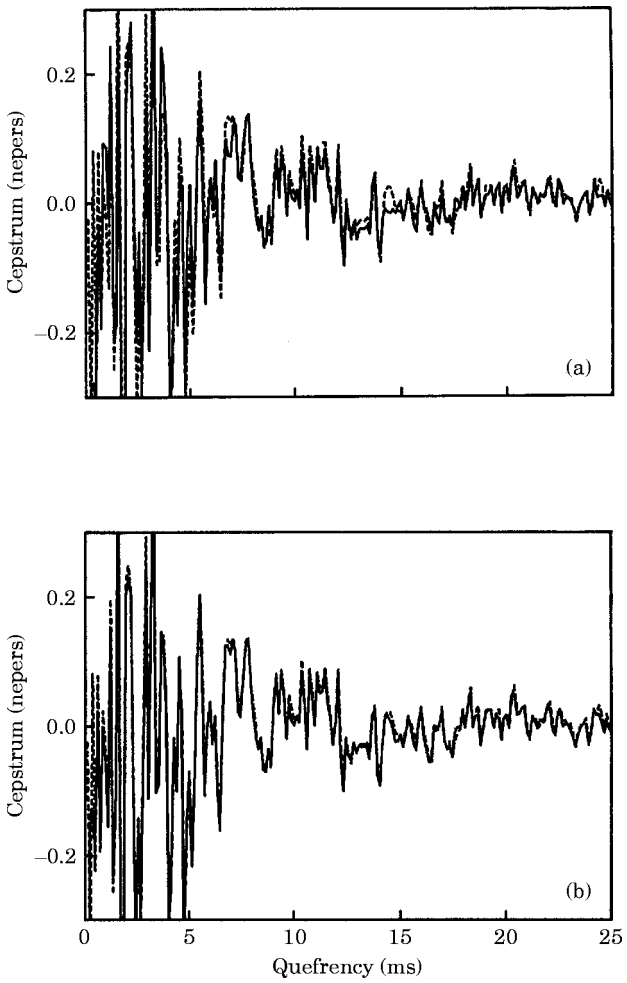

Figure 15. Cepstrum of measured FRF, – – –, and cepstrum regenerated from poles and zeros obtained by curve-fitting cepstrum of Fig. 14, ——. rahmonics removed by (a) sine squared weighting function and (b) comb weighting function.

5. CONCLUSIONS

An externally measured vibration signal is the convolution of the sampled impulse response of the path with the sampled source signal in discrete digital signal processing. After transformation to the cepstrum domain, the source and the path effects are deconvolved and become additive. For many practical applications, such as sources with reasonable flat autospectra and/or repeating events, the sources are highly concentrated at low quefrency and/or in discrete rahmonics in the cepstrum domain. The remainder of the quefrency regions are dominated by the path cepstra which can be approximated by the complex conjugate poles and zeros of the frequency response function.

A NLLS procedure, the Levenberg–Marquardt method, and the ITD method have been adapted and applied to curve-fit the quefrency regions dominated by the path cepstra. In the curve-fitting procedure, the source cepstra can be removed by liftering operations and the poles and zeros are extracted by curve-fitting the path dominated complex or differential cepstra to their analytical expression. In the NLLS procedure, both the initial positions and the number of poles and zeros need to be specified, which often can be

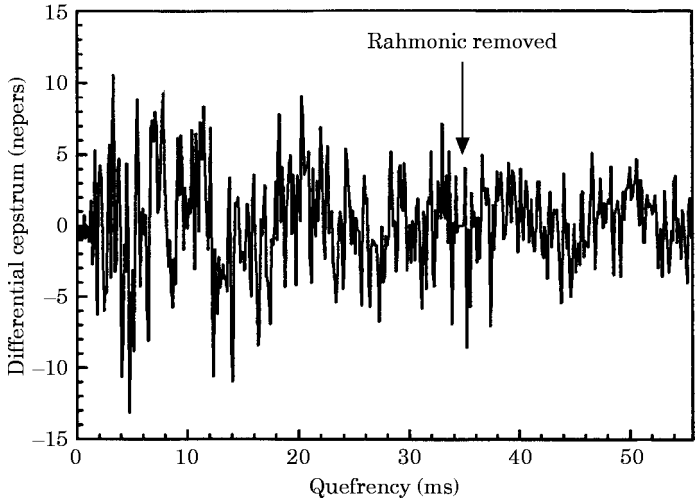

Figure 16. The response differential cepstrum (driving point) under a double impact excitation with rahmonics removed.

obtained by directly reading from the measured auto spectrum. The NLLS procedure can be applied to both complex and differential cepstra. It was found that with the latter, a larger quefrency range of the differential cepstrum data set (in comparison with the corresponding complex cepstrum data set) can be used for the purpose of extracting poles and zeros. Compared with the NLLS procedure, the ITD method has the advantages that neither the number, nor the initial positions of the poles and zeros are required in advance. However, differential cepstra measured at multiple points are necessary in order to separate the poles and zeros, both of which are identified as 'modes' in the ITD method.

The response signals from a free–free beam were used and the excitations (sources) were hammer blows. By using an appropriate hammer tip, it can be ensured that the spectrum of the forcing function is relatively smooth and flat, and thus the source complex (and differential) cepstra are concentrated within a very short low quefrency section. Then, the additional complication of a double impact was introduced, thus adding a series of

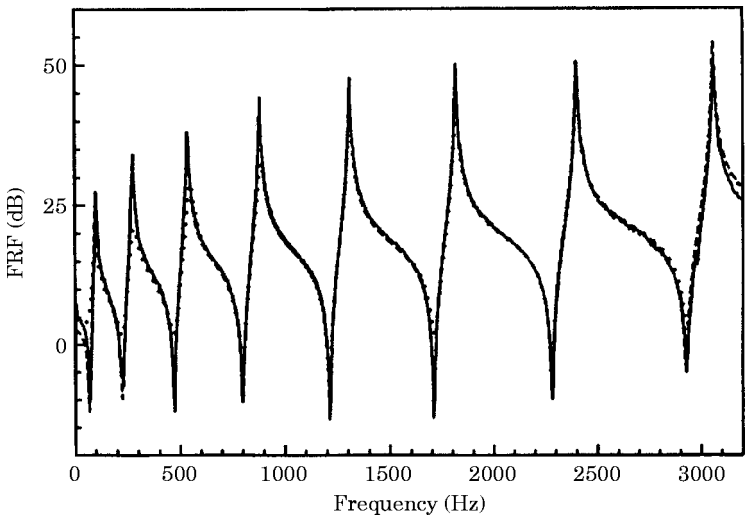

Figure 17. Comparison of results for ITD method (. . . .) with NLLS (– – –) and direct measurement (——).

rahmonics at higher quefrencies, and simulating the situation in gear and other periodic vibrations. In both cases, all the results, obtained by means of the following methods, the NLLS procedure, the ITD method, a rational fraction polynomial curve fitter and measurements, correspond well and indicate that the method could be applied to a wider range of applications where the basic assumptions are satisfied. Part II [20] discusses the regeneration of FRFs from the identified poles and zeros in the frequency band of interest.

ACKNOWLEDGEMENTS

This research was supported by an Australian Research Council grant.

REFERENCES

1. B. P. Bogert *et al*. 1963 *Proceedings of the Symposium on Time Series Analysis*. M. Rosenblatt (ed.), pp. 209–243. The frequency analysis of time series for echoes: cepstrum, pseudo-auto covariance, cross cepstrum, and saphe cracking. New York: John Wiley.
2. S. Aatola *et al*. 1990 *Noise Control Engineering Journal* **34**(2), 53–59. Cepstrum analysis predicts gearbox failure.
3. P. Bradshaw and R. B. Randall 1983 *Mechanical Signature Analysis*. S. Braun (ed.), pp. 7–17. Early detection and diagnostics of machine faults on trans Alaska pipeline. New York: ASME.
4. J. H. Derby 1978 *IEEE International Conference on Acoustics*, *Speech*, *and Signal Processing*, Tulsa, OK, pp. 214–217. Analysis and representation of composite signals by cepstral inverse filtering.
5. R. C. Kemerait 1987 *IEEE Southeast Conference '87*, ch. 2398–6, 256–259. A new cepstral approach for prognostic maintenance of cyclic machinery.
6. N. Khalili and R. Leskinen 1990 *Proceedings of IEEE ICASSP*, pp. 2423–2426. Cepstral analysis with dispersion.
7. J. T. Kim and R. H. Lyon 1992 *Mechanical Systems and Signal Processing* **6**, 1–15. Cepstral analysis as a tool for robust processing, deverberation and detection of transients.
8. R. H. Lyon 1987 *Machinery Noise and Diagnostics*. London: Butterworths.
9. R. H. Lyon and J. T. Kim 1988 *Robotics and Computer-Integrated Manufacturing* **4**, 447–455. Reduced parameter set descriptions for system and event identification.
10. C. L. Nikias and R. Pan 1988 *IEEE Transactions on Acoustics*, *Speech and Signal Processing* **36**, 1706–1714. Time delay estimation in unknown Gaussian spatially correlated noise.
11. R. B. Randall and Y. Gao 1991 *Proceedings of the 1991 Asia-Pacific Vibration Conference*. *Monash University*, *Melbourne*, *Australia*, pp. 1, 2.12–2.17. Extraction of the modal parameters from the response autospectrum.
12. R. B. Randall, Y. Gao and A. Sestieri 1994 *Mechanical Systems and Signal Processing* **8**, 607–622. Phantom zeros in curve-fitted frequency response functions.
13. R. B. Randall 1980 *Proceedings of the Institute of Mechanical Engineers Conference on Vibration in Rotating Machinery*, Cambridge, MA, pp. 169–174. Advances in the application of cepstrum analysis to gearbox diagnosis.
14. R. B. Randall 1982 *ASME Transactions: Journal of Mechanical Design* **104,** 259–267. A new method of modeling gear faults.
15. R. B. Randall 1984 *Proceedings of the Institute of Mechanical Engineers Conference on Vibration in Rotating Machinery*, York, pp. 101–107. Separating excitation and structural response effects in gear-boxes.
16. A. V. Oppenheim and R. W. Schafer 1989 *Discrete Time Signal Processing*. Englewood Cliffs, NJ: Prentice-Hall.
17. R. B. Randall 1987 *Frequency Analysis*, 3rd edn. Naerum, Denmark: Bruel and Kjaer.
18. T. Berther and P. Davies 1991 *Tribology Transactions* **34,** 321–326. Condition monitoring of check valves in reciprocating pumps.
19. J. E. Dennis and R. B. Schnabel 1983 *Numerical Methods for Unconstrained Optimistion and Nonlinear Equations*. Englewood Cliffs, NJ: Prentice-Hall.
20. Y. Gao and R. B. Randall 1996 *Mechanical Systems and Signal Processing*. Determination of frequency response functions from response measurements. II—Regeneration of frequency response functions from poles and zeros **10**, 319–340.

21. S. R. Ibrahim 1978 *Journal of Spececraft and Rockets (AIAA)* **15** (Sept.–Oct.). 313–316. Modal confidence factor in vibration testing.
22. R. S. Pappa and S. R. Ibrahim 1981 *The Shock and Vibration Bulletin* **51,** 43–72. A parametric study of the Ibrahim time domain identification algorithm.
23. R. B. Randall and Y. Gao 1994 *Journal of Sound and Vibration* **176,** 179–193. Extraction of modal parameters from the response power cepstrum.
24. J. M. Tribolet 1977 *IEEE Transactions on Acoustics, Speech, and Signal Processing* **25,** 170–177. A new phase unwrapping algorithm.
25. R. Pan and C. L. Nikias 1988 *IEEE Transactions on Acoustics, Speech, and Signal Processing* **36,** 186–205. The complex cepstrum of higher order cumulants and nonminimum phase system identification.
26. A. Polydoros and A. T. Fam 1981 *Proceedings of IEEE International Symposium on Circuits Systems*, 77–80. The differential cepstrum: definition and properties.
27. A. M. Abel-Ghaffer and G. W. Housner 1978 *Journal of the Engineering Mechanics Division, ASCE 104(EM5)*. Ambient vibration test of suspension bridge.
28. R. D. Begg *et al*. 1976. *Proceedings of the Offshore Technology Conference OCT 2549 2*. Structural integrity monitoring using digital processing of vibration signals.
29. J. S. Bendat and A. G. Piersol 1980 *Engineering Applications of Correlation and Spectral Analysis*. New York: John Wiley.
30. Y. Gao 1994 *PhD Dissertation*. University of New South Wales, Australia. Extraction of modal parameters from response vibrations.
31. Y. Gao and R. B. Randall 1992 *Proceedings of the 17th International Seminar on Modal Analysis*, K. U. Leuven, Belgium, pp. 1643–1654. Zeros vs residues.
32. D. J. Ewins 1989 *Modal Testing: Theory and Practice*. Letchworth: Research Studies Press.
33. S. R. Ibrahim and E. C. Mikulcik 1977 *The Shock and Vibration Bulletin* **47,** 183–198. A method for the direct identification of vibration parameters from the free response.
34. S. R. Ibrahim 1984 *AIAA Proceedings of the 25th Structures, Structural Dynamics and Materials Conference*, Paper 84-0928, pp. 117–122. A modal identification algorithm for higher accuracy requirements.
35. S. R. Ibrahim 1986 *AIAA Journal* **24,** 499–503. Double least square approach for use in structural modal identification.
36. R. B. Randall and Y. Gao 1993 *Proceedings of the Conference on Modern Practice in Stress and Vibration Analysis, Sheffield*, pp. 641–653. Adaptation of the ITD method to the extraction of poles and zeros from the response cepstrum.
37. Y. Gao *et al*. 1987 *Journal of Vibration and Dynamic Measurements* 1–5. Mode shape coherence and confidence factor. (In Chinese.)
38. Y. Gao 1989 *Journal of Mechanical Strength* **11**(2), 61–65. An improved ITD method. (In Chinese.)
39. Y. Gao 1991 *Proceedings of the 1991 Asia-Pacific Vibration Conference, Monash University, Melbourne*, 1, 2.78–2.83. Zoom analysis in the Z-plane.
40. G. M. Lee and M. W. Trethewey 1989 *Mechanical Systems and Signal Processing* **3**, 425–435. Modal parameter separation for oversized finite difference time domain models.

APPENDIX A: NON-LINEAR LEAST SQUARES OPTIMISATION

The error function to be minimised in our case is represented by equations (13) and (14) which are reproduced here:

$$e(\beta, n) = \hat{x}(n) - \hat{h}(n)$$

$$= \hat{x}(n) - 2\sum_{k=1}^{N_i/2} \frac{1}{n}\beta_{2k-1}^{n} \cos(\beta_{2k} n) + 2\sum_{k=1}^{M_i/2} \frac{1}{n}\beta_{P_i+2k-1}^{n} \cos(\beta_{P_i+2k} n) \tag{13}$$

where the corresponding variable vector to be extracted can be constructed as:

$$\beta = [A_{c1}, \omega_{c1}, A_{c2}, \omega_{c2}, \ldots, A_{cP_i/2}, \omega_{cP_i/2}, A_{a1}, \omega_{a1}, A_{a2}, \omega_{a2}, \ldots, A_{aM_i/2}, \omega_{aM_i/2}]^T$$

$$= [\beta_1, \beta_2, \ldots, \beta_{P_i+M_i}]^T. \tag{14}$$

The non-linear least squares problem consists of choosing β so that the fit is as close as possible in the sense that the sum of the squares of the errors $e(\beta, n)$ is minimised. Here, the Levenberg–Marquardt approach is recommended, which chooses β by solving the following minimisation problem [20]:

$$\underset{\beta_{k+1}\in\mathscr{R}^p}{\text{minimize}} \| E(\beta_k) + J(\beta_k)(\beta_{k+1} - \beta_k) \|_2 \tag{A1}$$

$$\text{subject to: } \| \beta_{k+1} - \beta_k \| \leqslant \delta_k$$

where

$$E(\beta)^T = [\hat{x}(1) - \hat{h}(\beta, 1), \hat{x}(2) - \hat{h}(\beta, 2), \ldots, \hat{x}(m) - \hat{h}(\beta\, m)] \tag{A2}$$

is a vector of the error function of equation (13), and:

$$J(\beta)_{ij} = \frac{\partial e_i(\beta)}{\partial \beta_j} \tag{A3}$$

is the first derivative matrix (Jacobian) of $E(\beta)$, or

$$\begin{cases} J_j(\beta, n) = -2\beta_j^{n-1} \cos(\beta_{j+1} n) \\ J_{j+1}(\beta, n) = 2\beta_j^n \sin(\beta_{j+1} n) \end{cases} \quad j = 2r - 1,\ r = 1, 2, \ldots, P_i/2$$

$$\begin{cases} J_j(\beta, n) = 2\beta_j^{n-1} \cos(\beta_{j+1} n) \\ J_{j+1}(\beta, n) = -2\beta_j^n \sin(\beta_{j+1} n) \end{cases} \quad j = P_i + 2r - 1,\ r = 1, 2, \ldots, M_i/2 \tag{A4}$$

where subscript k represents the number of the iteration. The Levenberg–Marquardt algorithm requires initial trial values of the variable vector, β, which is to be extracted and the exact order of the model function, $f(\beta, n)$, (in our case the number of poles and zeros).

Where the differential cepstrum is used in place of the complex cepstrum, the variable vector extracted is the same as in equation (14) and the Jacobian matrix, equation (A3) multiplied by the quefrency index n.